PRAMANA
— journal of
physics

Vol. 77, No. 5
November 2011
pp. 987–1005

Flip-flop between soft-spring and hard-spring bistabilities in the approximated Toda oscillator analysis

B K GOSWAMI

Laser and Plasma Technology Division, Bhabha Atomic Research Centre, Mumbai 400 085, India
E-mail: binoy@barc.gov.in

Abstract. We study theoretically the effect of truncating the nonlinear restoring force ($\exp(\Phi)-1 = \sum_{n=1}^{\infty}\Phi^n/n!$) in the bistability pattern of the periodically driven, damped one-degree-of-freedom Toda oscillator that originally exhibits soft-spring bistability with counterclockwise hysteresis cycle. We observe that if the truncation is made third order, the harmonic bistability changes to hard-spring type with a clockwise hysteresis cycle. In contrast, for the fourth-order truncation, the bistability again becomes soft-spring type, overriding the effect of third-order nonlinearity. Furthermore, each higher odd-order truncation attempts to introduce hard-spring nature while each even-order truncation turns to soft-spring type of bistability. Overall, the hard-spring effect of every odd-order nonlinear term is weaker in comparison to the soft-spring effect of the next even-order nonlinear term. As a consequence, higher-order approximations ultimately converge to the soft-spring nature. Similar approximate analysis of Toda lattice has in recent past revealed remarkably similar flip-flop pattern between stochasticity (chaotic behaviour) and regularity (integrability).

Keywords. Toda oscillator; Duffing oscillator; soft-spring and hard-spring bistabilities; principle of harmonic balance; Hamiltonian chaos; integrability; Toda lattice.

PACS Nos 05.45.Ac; 05.45 Gg; 05.45 Pq

In the course of analytical studies (e.g., perturbation analysis of a dynamical system), researchers commonly truncate some or other complex expansions in the respective theoretical model for convenience. On the condition that no significant qualitative change would occur in the given operating regime if higher-order nonlinear terms are taken into account. However, in many an occasion, it has also been observed that increasing the order of approximation just once may lead to a contrasting scenario. For instance, we cite the classic example of Contopoulos and Polymilis [1] who have numerically analysed the effect of finite-order approximation of the exponential potential in three-particle Toda lattice [2]. When the potential is truncated at third order, the model is reduced to Henon and Heiles (HH) Hamiltonian. Thus, while the original Toda Hamiltonian is integrable, the third-order approximation can exhibit chaotic dynamics. Contopoulos and Polymilis have investigated in great detail the transition from chaotic HH Hamiltonian to integrable Toda model, by increasing higher-order terms sequentially, and observed a very interesting

DOI: 10.1007/s12043-011-0199-8; ***e*Publication: 31 October 2011**

pattern: The dynamics of third- and fourth-order approximated models are in sharp contrast. For instance, for a large range of energy, when the third-order approximation is chaotic, fourth order shows regular behaviour. Furthermore, for all the odd-order approximations, the dynamics is qualitatively similar to the HH case. It appeared in some sense that, for a given energy, odd-order terms tend to make the system chaotic while even-order terms attempt to induce order or integrability. Even-order terms dominate and as a result, asymptotically, the integrability prevails. In the intermediate regime of approximation, one may notice a flip-flop pattern between chaotic and regular dynamics. Similar truncation analysis has been made by others [3,4] including with a perturbed HH Hamiltonian [5] and with the sixth-order truncation of Toda Hamiltonian [6].

In this paper, we are interested to inquire in what way the approximated nonlinear systems will behave if similar truncations were carried out in the dissipative limit. We consider the class of one-degree-of-freedom nonlinear oscillators for simplicity. It is well-known that subject to the symmetry of the potential and nonlinearity of damping, these oscillators go to some or other equilibrium states or even exhibit Hopf bifurcation but cannot become chaotic. To make them chaotic, the dimension requires an enhancement, typically by some (quasi)periodic force (parametric excitation), delayed feedback etc. In this paper, we concentrate on periodic driving. In weak driving, the oscillator shows harmonic resonance that is symmetric as in a simple harmonic oscillator. When the drive amplitude is increased further, harmonic resonance exhibits bistability and various subharmonic resonances occur, as observed in Duffing, Morse, Toda oscillators [6a], and gravitational pendulum in particular, and the periodically driven nonlinear systems in general. Typically, there are two types of bistabilities, soft-spring and hard-spring types [6b]. We illustrate this feature further through the schematic bifurcation diagrams of harmonic bistability in figure 1. The vertical coordinate X represents any suitably sampled dynamical variable, say the stroboscopic projection with sampling frequency the same as the driving frequency. In each panel, the solid lines AB and CD refer to stable period-1 states while the broken line BC refers to the unstable period-1 state. In soft-spring bistability (figure 1a), the upper turning point 'C' is inclined towards low-frequency side. In some loose yet popular sense of mechanical vibration, the inclination towards low-frequency side may be thought of as the reduction of the resonance frequency due to reduced stiffness ('softening effect' in some sense). The associated jumps due to inverse saddle-node bifurcations from the points 'B' and 'C' (shown by straight arrows) lead to counterclockwise hysteresis. In contrast, in hard-spring bistability (figure 1b), the upper turning point 'B' is inclined towards high-frequency side that again may be thought off as due to the increase of stiffness. Also, the hysteresis cycle is clockwise. Typically, in a symmetric Duffing oscillator, the sign of the cubic nonlinearity in the restoring force determines the nature of bistability [14]. If it is positive, bistability is hard-spring type. In contrast, if it is negative, the bistability is soft-spring type. It would therefore be interesting to explore whether finite orders of approximation of restoring force lead to any qualitative changes in the type of bistability. In this paper, we indeed show a fascinating flip-slop scenario with Toda oscillator model of class-B lasers. The oscillator equation can be written in the following form:

$$\ddot{\Phi} + \alpha\dot{\Phi}\left[1 + c\,(\exp(\Phi) - 1)\right] + [1 - m\cos(\omega\tau)](\exp(\Phi) - 1) = F\cos(\omega\tau + \vartheta), \tag{1}$$

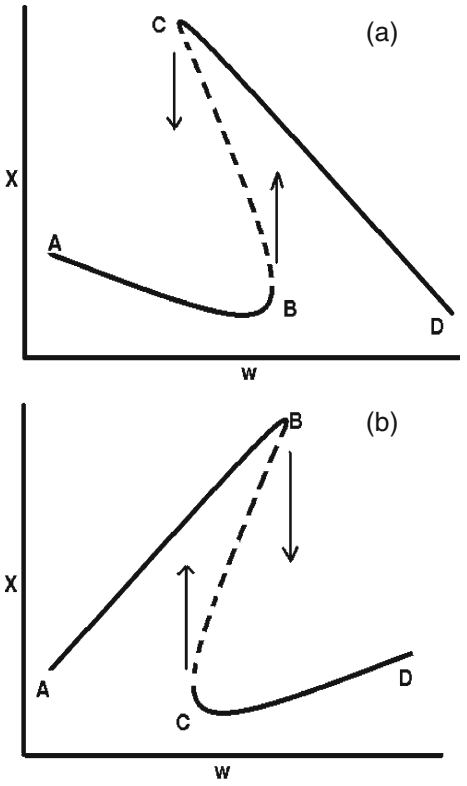

Figure 1. Schematic bifurcation diagram of typical harmonic bistability patterns. The vertical coordinate X represents a suitably sampled (say stroboscopically) dynamical variable and the horizontal coordinate is the driving frequency. The turning points B and C represent saddle-node bifurcation conditions. (**a**) Typical soft-spring bistability pattern. The upper turning point is located at the low-frequency side and the hysteresis cycle is anticlockwise. (**b**) Typical hard-spring bistability scenario. The upper turning point is located at the high-frequency side and the hysteresis cycle is clockwise.

where

$$F = \frac{m\sqrt{\left(\omega^2\Omega^2 + \epsilon^2\right)}}{\epsilon - 1},$$

and

$$\vartheta = \tan^{-1}(\omega\Omega/\epsilon)\,.$$

The laser intensity $I = I_0 \exp(\Phi)$ where $I_0 = \epsilon - 1$ is the laser intensity in the absence of any cavity-loss modulation and ϵ is the pump parameter. The cavity-loss $k = k_0(1 + m\cos(\omega\tau))$ and the relaxation oscillation frequency $\Omega = \sqrt{k_0(\epsilon - 1)}$. The dissipativity $\alpha = \epsilon/\Omega$ and $c = (\epsilon - 1)/\epsilon$. From eq. (1), one can also notice that the resonance frequency $\omega_r = 1$.

The complexity of the oscillator dynamics depends on the operating regime. We consider the following parameter values as an example: $k_0 = 1.5 \times 10^4, \epsilon = 2, \alpha = 0.015$ and

observe that a modulation depth as small as 0.005 requires many higher-order terms of the exponential series for the convergent behaviour. Let us define the period-1 solution of eq. (1) as follows:

$$\Phi_e = A_0 + A_1 \cos(\omega\tau + \xi_1) + A_2 \cos(2\omega\tau + \xi_2). \tag{2}$$

On the basis of the FFT analysis of the period-1 solution at various values of the drive amplitude, we notice that eq. (2) is a good approximation in the parameter regime ($m < 0.00035$). Therefore, to describe the convergence process in the harmonic bistability semi-analytically, we consider $m = 0.0003$. Next we approximate the exponential functions in the damping and restoring force terms in finite series. Following the principle of harmonic balance method [15], we substitute eq. (2) into (1), and equate constant terms, coefficients of $\cos(\omega\tau)$, $\sin(\omega\tau)$, $\cos(2\omega\tau)$, $\sin(2\omega\tau)$ from both sides of eq. (1). Finally, we derive a system of five coupled nonlinear algebraic solutions [15a]. By solving these equations numerically, we compute the frequency response of the harmonic amplitude A_1 for various orders of approximations of the exponential function in the restoring force term. These response curves may be considered as the representatives of the actual bifurcation diagrams. Every turning point in the response curve represents a saddle-node bifurcation. Figure 2a shows the frequency responses for various orders of truncation in the restoring force of eq. (1). The exponential function in the damping term is approximated up to sixth order which is found to be satisfactory. Curve (a) shows the frequency response in the case of third-order approximation. Let the driving frequency of the upper turning point be denoted by ω_{s3} where the suffix 's' stands for saddle-node bifurcation and '3' stands for third-order approximation. We notice that third-order approximation exhibits hard-spring bistability with $\omega_{s3} > \omega_r$. In contrast, when we consider the fourth-order approximation, the bistability is soft-spring type, as seen from the frequency-response curve (b). We denote the driving frequency for the upper saddle-node bifurcation by ω_{s4} where the suffix 's' stands for saddle-node bifurcation and '4' stands for fourth-order approximation. From curve (b) we may notice that $\omega_{s4} < \omega_r$. This means the fourth-order term overrides the hard-spring effect of the third-order term and exhibits soft-spring bistability. The curve (c) shows the frequency response for fifth-order approximation ($n = 5$). In this case, an overall convergence has been reached in the low-amplitude regime that attributes soft-spring pattern. However, the peak of the response curve is inclined again towards high-frequency side (in comparison to the fourth order approximation). This implies that the hard-spring effect of the fifth-order term could partially override the soft-spring effect of the fourth-order term even though there is a gradual convergence towards the soft-spring nature. Let us denote the drive frequency for the corresponding saddle-node bifurcation by ω_{s5} where the suffix 's' stands for saddle-node bifurcation and '5' stands for fifth-order approximation. From curve (c), we notice that $\omega_{s5} < \omega_{s3}$. Overall, this is an intermediate or mixed stage that exhibits soft-spring nature in the small A_1 regime and hard-spring nature at the peak. For the sixth-order approximation [curve (d)], the peak again swings to low-frequency side. However, the swing is much less than that in the case of fourth order. Following previous convention to identify the driving frequency of the upper turning point, we notice that $\omega_{s4} < \omega_{s6} < \omega_r$. Curve (e) refers to the frequency response curve for seventh-order approximation. In this case, the noticeable point is that peak of the curve has shifted towards low-frequency side; $\omega_{s6} < \omega_{s7} < \omega_r$. This implies that the odd-order

terms are no longer adequately strong to counterbalance the soft-spring effect of the even-order terms. The quantitative convergence of the soft-spring bistability is further endorsed from curve (f) that refers to eighth-order approximation. Thus, the limiting value of the drive frequency for the upper turning point will be within ω_{s7} and ω_{s8}. Figure 2a shows the numerically simulated bistability patterns (Y vs. ω) for various stages of approximation of restoring force. The damping function has been approximated at tenth order that is reasonably adequate. Y denotes the stroboscopically sampled asymptotic fixed points of Φ; sampling frequency equals to ω. Coloured curves (a)–(f) show the bifurcation diagrams for $n = 3, 4, \ldots, 8$ respectively. For even values of n; $n = 4, 6, 8$, the bistability is soft-spring type with the upper turning point $\omega_s < \omega_r$. For $n = 3$, the bistability is hard-spring type with $\omega_s > \omega_r$. For $n = 5$, an overall convergence has been reached in the low-amplitude regime that resembles soft-spring pattern. However, the peak is still tilted towards right-hand side. Therefore, this is an intermediate or mixed stage between soft- and hard-spring type. From $n = 7, 8$ onwards, the bistability pattern appears convergent to a soft-spring scenario. Thus the results of semi-analytical studies have been endorsed by the numerically simulated results.

Having investigated the effect of approximation of the exponential function in the restoring force, it may also be interesting to know what is the effect of similar approximation of the exponential function in the damping term in eq. (1). We continue the semi-analytical studies of harmonic resonance with unchanged values of oscillation parameters. The restoring force is approximated up to eighth order which is found to be satisfactory. Figure 3a shows the results for various stages of approximation of the nonlinear damping function in eq. (1). Curves (a), (b), (c) and (d) respectively denote the $n = 3, 4, 5$ and 6th order of approximation. Here again one notices another type of flip-flop pattern, namely the location of the upper turning point goes up and down. The height of the peak along the inclined tongue is highest for third-order approximation and lowest for fourth order. As we improve the approximation, the location of the peak converges somewhere in between. We may remark that the presence of exponential function in the damping term enhances the dissipativity and therefore raises the onset of subharmonic bifurcations or chaos. Also notice that various stages of approximation in the damping term do not change the qualitative nature of bistability as it is always soft-spring type. Similar features have been confirmed by the numerical integration of eq. (1). For instance, figure 3b shows the bistability patterns at various stages of approximation of nonlinear damping function. One would notice that for odd values of n; $n = 3, 5$, the peak of the response curve goes up. In contrast, for even orders of approximation, the peak comes down. The limiting scenario is close to sixth-order approximation.

To investigate in more detail the mixed stage of harmonic stability, we analyse the harmonic resonance at a relatively large modulation depth $m = 0.001$. Figure 4 illustrates a few numerically simulated bifurcation diagrams for various stages of approximation in the nonlinear restoring force. In figure 4a, we show the third (violet circles) and fourth (green curve) order approximations. Third-order approximation exhibits hard-spring bistability and clockwise hysteresis, as evident in the bistable region '1234'. In contrast, the fourth-order approximation has a very narrow bistable region (not prominently visible) that exhibits soft-spring behaviour. The peak height is also relatively small. Next, we have included the higher-order nonlinear terms sequentially up to 20th order. The bifurcation pattern of the approximated models can be divided into two groups – the even-order and

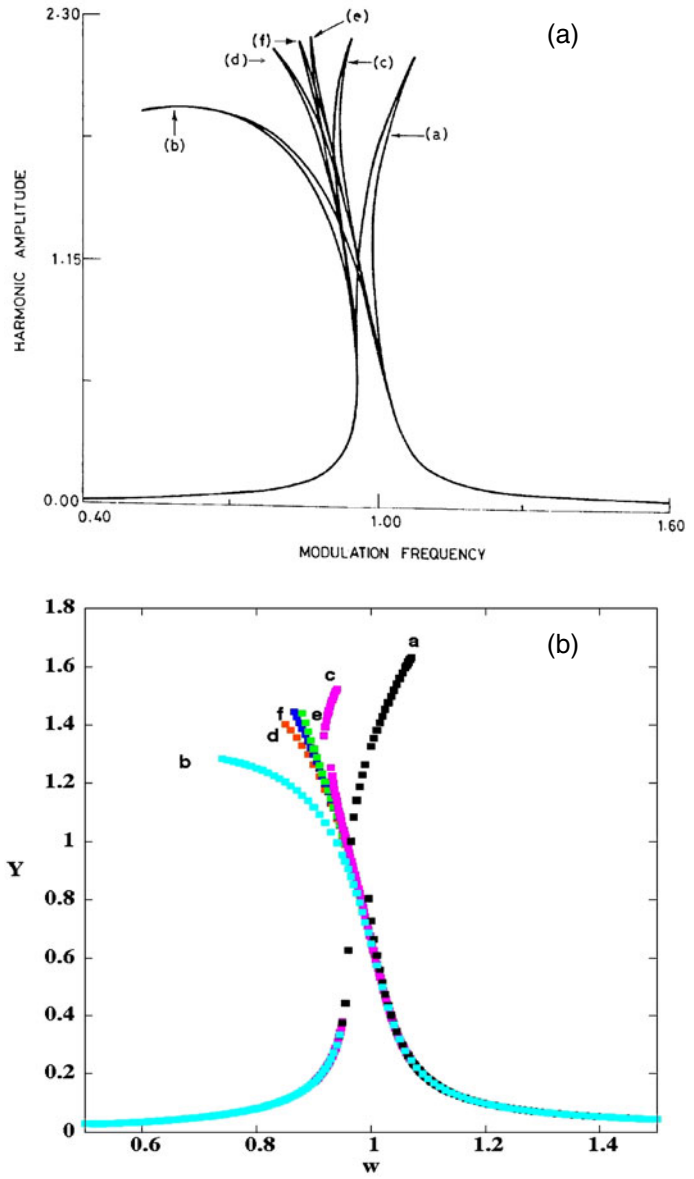

Figure 2. (**a**) Frequency response of the harmonic amplitude (A_1) for various stages approximation of the restoring force; $m = 0.0003$. Curves (a)–(f) show the frequency responses for $n = 3, 4, \ldots, 8$ respectively. (**b**) Numerically simulated bifurcation diagrams (Y vs. ω) for various stages of approximation of the restoring force; $m = 0.0003$. The coloured curves (a)–(f) show the bifurcation diagrams for $n = 3, 4, \ldots, 8$ respectively. The coloured symbols of the bifurcation diagrams are defined as follows: (black) $n = 3$; (light blue) $n = 4$; (pink) $n = 5$; (orange) $n = 6$; (green) $n = 7$ and (blue) $n = 8$.

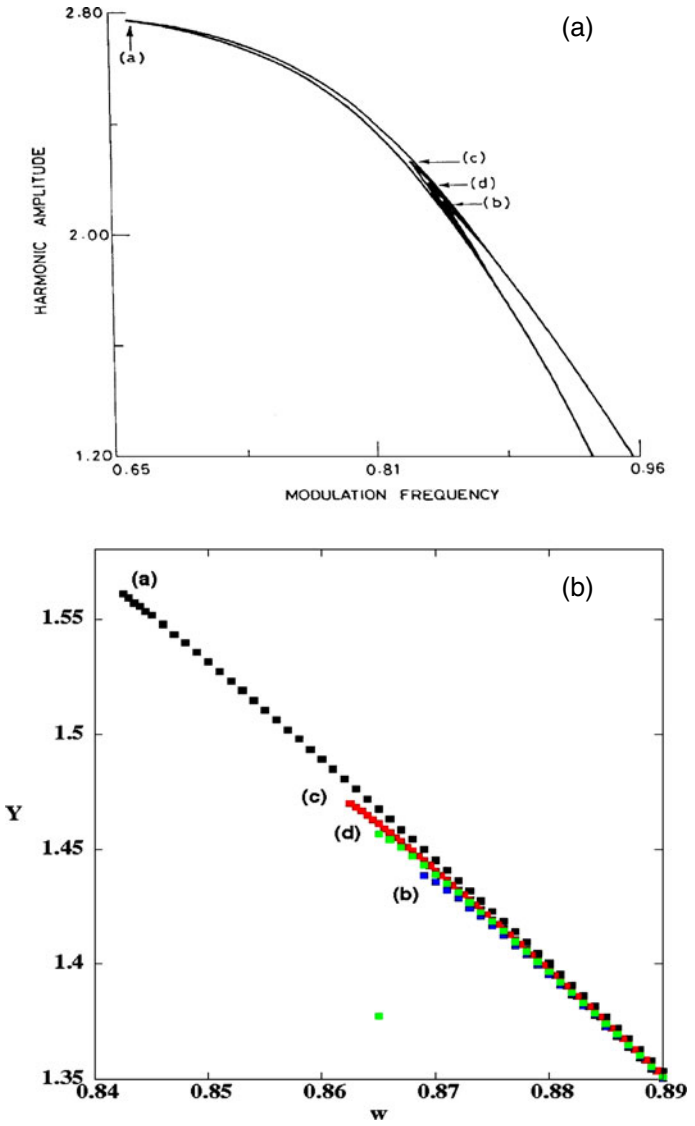

Figure 3. (**a**) Frequency response of the harmonic amplitude (A_1) for various stages of approximation of the nonlinear damping function; $m = 0.0003$. Curves (a)–(f) show the frequency responses for $n = 3, 4, 5, 6$ respectively. (**b**) Numerically simulated bifurcation diagrams (Y vs. ω) for various stages of approximation of the nonlinear damping function; $m = 0.0003$. The coloured symbols of the bifurcation diagrams are defined as follows: (black) $n = 3$; (blue) $n = 4$; (red) $n = 5$, (green) $n = 6$.

the odd-order approximations. To explain further, we present some selected cases as examples. In figure 4b we show seventh (blue curve) and eighth (red curve) order approximations. In seventh-order approximation, the hysteresis cycle '3456' is clockwise with

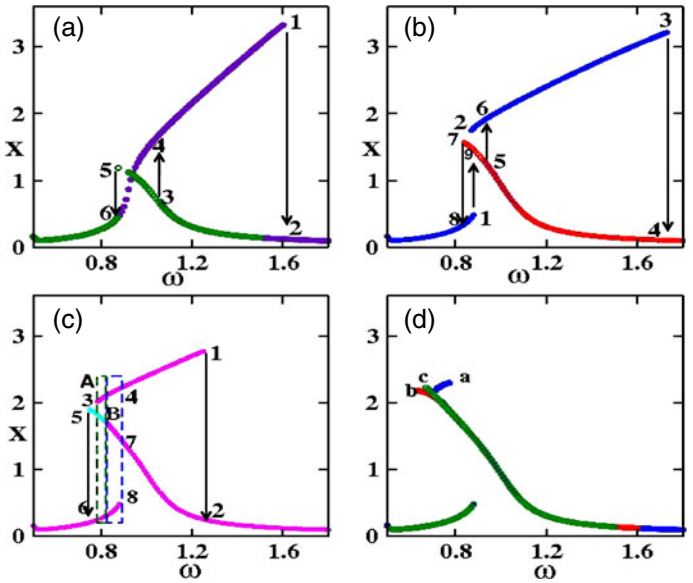

Figure 4. Bifurcation diagrams in the harmonic resonance for various stages of approximation in the nonlinear restoring force; $m = 0.001$. (**a**) Third- (violet curve) and fourth- (green curve) order approximations. (**b**) Seventh- (blue curve) and eighth- (red curve) order approximations. (**c**) Eleventh- (pink curve) and twelfth- (light blue curve) order approximations. The bistable region is within the green segmented box 'A' and the tristable region is in blue segmented box 'B'. (**d**) Fifteenth- (blue curve), sixteenth- (red curve) and twentieth- (green curve) order of approximations.

hard-spring bistability. However, in comparison to the gradual rise from the point '6' to '4' (in the period-1 branch) in the third-order approximation, the seventh-order approximation exhibits a sharp rise from point '1' (in the small-amplitude period-1 branch) to the point '2' in the large amplitude period-1 branch. Eighth-order approximation again shows a pattern, similar to $n = 4$ and opposite to $n = 7$ order approximation. The upper turning point has gone up and there is a distinct bistable region '1978' with counterclockwise hysteresis cycle. In figure 4b, we show the eleventh-order (pink curve) and twelfth-order (light blue curve) approximations. Eleventh-order approximation still has a '1274' hysteresis cycle with hard-spring bistability. However, the softening effect is also much more prominent, resulting in a bistable region (within the green segmented box A) and a tristable region (within the blue segmented box B). Thus, we find a mixed nature where one cannot attribute a unique pattern. In contrast, the twelfth-order approximation is qualitatively similar to the eighth-order approximation. Here again, the upper turning point has gone up further and there is a relatively large bistable region '8756' with counterclockwise hysteresis cycle. As we improve the order of approximation, this intermediate behaviour for odd-order approximations gradually get transformed to pure soft-spring bistability with a gradual disappearance of hard-spring bistable region. This would be imperative in figure 4d where we show the 15th order (blue curve), 16th order (red curve) and 20th order (green curve) of approximations. From figure 4a–4d one can notice that the upper turning point of

the odd-order approximations is steadily coming down and the hard-spring bistable interval is also reducing. In contrast, soft-spring bistable window is increasing and the upper turning point is also rising. Also, in the convergent scenario ($n = 20$), the tristability has disappeared. Thus we notice that all even-order nonlinear terms attempt to introduce soft-spring bistability. In contrast, all odd-order terms attempt hard-spring bistability. The overall convergence exhibits soft-spring bistability.

Next we investigate the effect of truncation of the nonlinear restoring force in the period-2 subharmonic resonance phenomenon. We consider a relatively large magnitude of the driving amplitude ($m = 0.001$). Figure 5 illustrates the associated subharmonic bistability patterns. The nonlinear damping function has been approximated at $n = 10$ that has been found adequate. Figure 5a shows the case of third-order approximation in the restoring force. The typical scenario is as follows: If we reduce the driving frequency from $\omega > 2$, the system exhibits supercritical period doubling at the point '1' and remains in the period-2 state till it undergoes an inverse period-2 saddle-node bifurcation at point '2' and then the system jumps to the point '3' in a coexisting large-amplitude period-2 branch. When we decrease ω further, the system remains at the large-amplitude period-2 branch till it undergoes another inverse saddle-node bifurcation (at the point '4') that leads the system to another period-1 branch (at the point '5'). If we increase ω thereafter, the system remains at the period-1 state till it undergoes subcritical period doubling (at point '6') and subsequently, the system jumps back again at the point '7' on the large-amplitude period-2 branch. If the frequency is increased steadily, there will be another inverse saddle-node bifurcation at the point '8' when the system will jump down to the period-1 branch at the point '9'. Note that the points '1' and '6' are the boundaries of the period-2 subharmonic resonance region. Also, the points '4' and '6' are connected by a period-2 saddle (schematically shown by a blue solid curve). Similarly, the points '2' and '8' are connected by another period-2 saddle (schematically shown by a blue solid curve). The orbit structure, that connects the '6', '4', '8', '2' and '1' points, describe the period-2 subharmonic resonance. In this structure, the low-amplitude regime '6421' is bent towards low-frequency side, a feature of a soft-spring oscillator. However, the peak '482' is bent towards the high-frequency side, a feature of a hard-spring oscillator. The low-amplitude regime has a bistable window '56' or '47' where the hysteresis cycle is counterclockwise. In contrast, the peak has another bistable window '38' or '219' that will have a clockwise hysteresis cycle. Thus, $n = 3$ order approximation is rich with hard-spring as well soft-spring bistable patterns. In contrast, $n = 4$ (shown in figure 5b) reveals a purely soft-spring bistability. Here, as we decrease frequency from the right-hand side of the period-2 resonance region, the period doubling is supercritical at the point '1' and the period-2, thus created, disappears at a lower frequency (at the point '2') via an inverse saddle-node bifurcation and the system jumps to the period-1 branch at the point '3'. If we increase ω further, the period-1 undergoes subcritical period doubling at the point '4' where the system jumps again back to the period-2 branch (at the point '5'). The period-2 saddle is schematically shown by the blue solid curve joining the points '2' and '4'. From the orbit structure '2345', one may notice a bistable interval '34' (or '25') where a period-1 state coexists in the phase space with a period-2. Also, the hysteresis cycle '4523' is counterclockwise. From these two stages of approximations, we notice that the odd order has both hard as well as soft-spring bistabilities. In contrast, the even-order approximation has only soft-spring bistability. Let us now increase the order of approximation sequentially

and see the qualitative evolution of the bistability patterns. In figure 5c, we have plotted the bifurcation diagrams for $n = 3, 4, 5, \ldots, 10$. Each bifurcation scenario is denoted by filled circles of a unique colour and the order of approximation is denoted at the respective upper turning point. For instance, the $n = 3$ case is shown by the maroon curve and the upper turning point is denoted by '3'. Similarly, $n = 4$ case is shown by green curve and the upper turning point is denoted by '4'. We notice that all the even orders behave in a very similar manner and reveal soft-spring bistability pattern with counterclockwise hysteresis cycle. In contrast, all odd orders also behave in a similar way but exhibit two bistable regimes, one soft-spring type and the other hard-spring. However, as the order of approximation increases, there is an overall convergence towards soft-spring pattern, a feature similar to the harmonic resonance.

Let us now look at these qualitative features in the perspective of those obtained earlier [1] by similar approximations of conservative Toda lattice:

(I) In the conservative case, the cubic approximation in the potential reduces the Toda Hamiltonian to Henon–Heiles Hamiltonian. In the dissipative case, cubic approximation in the restoring force leads to an asymmetric Duffing oscillator that exhibits hard-spring bistability in harmonic resonance, and both soft- as well as hard-spring bistabilities in period-2 subharmonic resonance regime.

(II) In the conservative case, the odd-order terms in the potential induce chaotic nature whereas the even-order terms induce order or integrability. As the order of approximation increases, the effect of the nonlinear terms reduces, irrespective of whether it is odd or even. The even-order terms are relatively stronger in comparison to the odd-order terms and the asymptotic Toda Hamiltonian is integrable. In the dissipative case, the odd-order terms in the restoring force induce hard-spring bistability. In contrast, the even-order terms induce soft-spring bistability. In this case as well, as the order of approximation increases, the effect of nonlinear terms reduces, irrespective of whether it is odd or even. The even-order terms are however relatively stronger in comparison to the odd-order terms and Toda oscillator is of soft-spring type [15b].

(III) In the conservative case, when the order of approximation is reasonably high, even-order approximations may also exhibit chaos. In the dissipative case, even-order approximation has not been found to give rise to hard-spring bistability. The odd-order approximations however exhibit simultaneous presence of hard- as well as soft-spring bistabilities in the intermediate regimes.

(IV) In the conservative case, the fourth-order approximation may be qualitatively a better candidate than the third-order one (i.e., HH) to represent Toda Hamiltonian. In the dissipative case, in a similar way, fourth-order truncation (with a suitable scaling of the fourth-order nonlinear term) may be preferable to the third-order truncation (Duffing oscillator) to represent Toda oscillator.

To conclude, we have demonstrated a flip-flop scenario between soft-spring and hard-spring bistabilities in Toda oscillator dynamics when the exponential function in the restoring force is approximated. The even-order terms create soft-spring bistability while the odd-order terms lead to hard-spring bistability. The even-order terms are stronger than the odd-order terms. As the order of approximation is increased, the effect of either type declines. The convergent nature of Toda oscillator is of soft-spring type. This flip-flop scenario between hard-spring and soft-spring bistabilities in dissipative Toda oscillator may have some analogy (in some sense) with flip-flop between stochasticity and regularity in

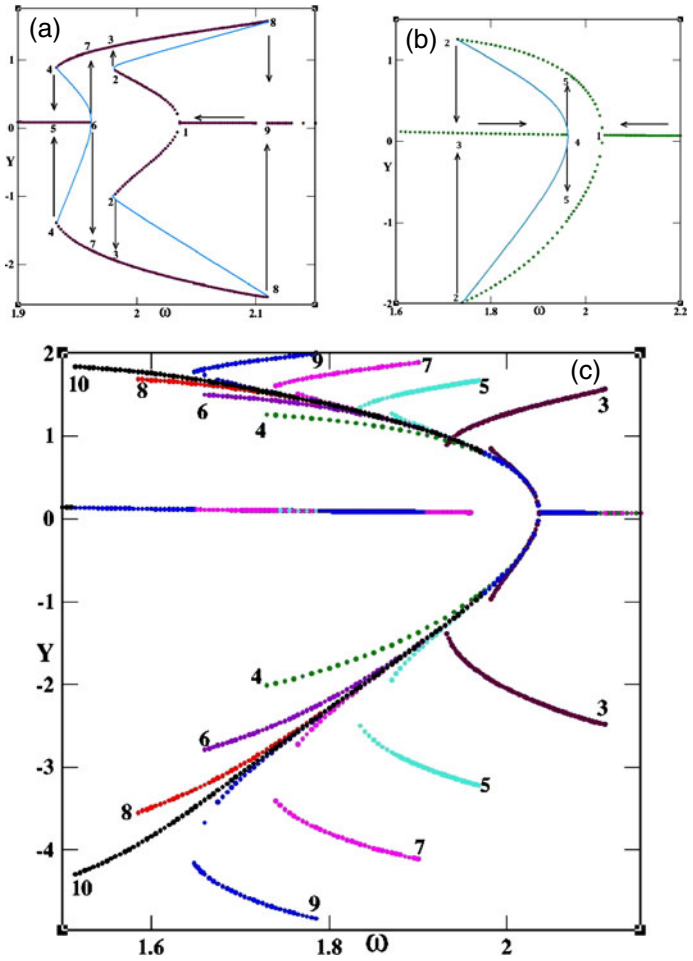

Figure 5. Bifurcation diagrams in the period-2 subharmonic resonance region for various stages of approximation in the nonlinear restoring force; $m = 0.001$. (**a**) Third-order approximation shows soft-spring as well as hard-spring bistabilities. (**b**) Fourth-order approximation shows soft-spring bistability. (**c**) The superposition of bifurcation diagrams for $n = 3, 4, \ldots, 10$ order of approximations.

the approximate analysis of Toda Hamiltonian for lattice vibration. A flip-flop scenario has also been observed when the exponential function in the damping term is approximated. In this case, the peak height oscillates between high and low values before converging somewhere in between.

Notice that we have studied the effect of finite-order approximation of the exponential function individually in the restoring force and the damping function. In order to do that, while studying the effect of restoring force function approximation, the damping function has been approximated adequately and vice varsa. Besides, the magnitude of the driving amplitude is small. The situation may be more complex if both the approximations are

of inadequate order and (or) the driving amplitude is relatively large. Finally, we may also remark that Morse oscillator is asymmetric and somewhat similar to Toda oscillator. Therefore, Morse oscillator is also expected to exhibit a similar flip-flop bistable scenario.

Appendix

Let

$$\Phi_e \equiv \Phi = A_0 + A_1 \cos\theta_1 + A_2 \cos\theta_2, \tag{1a}$$

where

$$\theta_1 = \omega\tau + \xi_1 \quad \text{and} \quad \theta_2 = 2\omega\tau + \xi_2. \tag{1b}$$

Let, Γ_{nlm} and Γ'_{nlm} denote the coefficients of $\cos(l\theta_1 + m\theta_2)$ in Fourier series of Φ^n and $(A_1\cos\theta_1 + A_2\cos\theta_2)^n$ respectively. For negative values of $l(m)$, a '$-$' sign is inserted before the respective $l(m)$ in the subscript of Γ_{nlm}. For instance, Γ_{32-1} denotes the coefficient of $\cos(2\theta_1 - \theta_2)$ in the Fourier series of Φ^3.

Fourier coefficients of Φ, Φ^2 and Φ^3:

$$\Gamma_{100} = A_0; \qquad \Gamma_{110} = A_1; \qquad \Gamma_{101} = A_2$$

$$\Gamma'_{200} = (A_1^2 + A_2^2)/2; \quad \Gamma_{200} = A_0^2 + \Gamma'_{200}; \quad \Gamma_{2-11} = A_1A_2$$

$$\Gamma_{210} = 2A_0A_1; \qquad \Gamma_{201} = 2A_0A_2; \qquad \Gamma_{220} = A_1^2/2$$

$$\Gamma_{32-1} = (3/4)A_1^2A_2; \quad \Gamma_{300} = A_0^3 + 3A_0\Gamma'_{200} + \Gamma_{32-1}\cos(2\xi_1 - \xi_2)$$

$$\Gamma'_{310} = (3/4)A_1^3 + (3/2)A_1A_2^2; \quad \Gamma_{310} = 3A_1A_0^2 + \Gamma'_{310}; \quad \Gamma_{3-11} = 3A_0\Gamma_{2-11}$$

$$\Gamma'_{301} = (3/4)A_2^3 + (3/2)A_2A_1^2; \quad \Gamma_{301} = 3A_2A_0^2 + \Gamma'_{301}; \quad \Gamma_{320} = (3/2)A_0A_1^2$$

$$\Gamma_{330} = A_1^3/4.$$

Fourier coefficients of Φ^4:

$$\Gamma_{42-1} = 4A_0\Gamma_{32-1}; \quad \Gamma'_{400} = (3/8)(A_1^4 + A_2^4) + (3/2)A_1^2A_2^2$$

$$\Gamma_{400} = A_0^4 + 6A_0^2\Gamma'_{200} + \Gamma'_{400} + \Gamma_{42-1}\cos(2\xi_1 - \xi_2)$$

$$\Gamma_{410} = 4A_0^3A_1 + 4A_0\Gamma'_{310}$$

$$\Gamma'_{4-11} = (3/2)A_1A_2(A_1^2 + A_2^2); \quad \Gamma_{4-11} = 6A_0^2\Gamma_{2-11} + \Gamma'_{4-11}; \quad \Gamma_{43-1} = A_1^3A_2/2$$

$$\Gamma'_{420} = A_1^4/2 + (3/2)A_1^2A_2^2; \quad \Gamma_{420} = 3A_0^2A_1^2 + \Gamma'_{420}; \quad \Gamma_{4-22} = (3/4)A_1^2A_2^2$$

$$\Gamma_{430} = 4A_0\Gamma_{330}; \quad \Gamma_{440} = A_1^4/8.$$

Fourier coefficients of Φ^5:

$$\Gamma'_{52-1} = (5/4)A_1^4A_2 + (15/8)A_1^2A_2^3; \quad \Gamma_{52-1} = 10A_0^2\Gamma_{32-1} + \Gamma'_{52-1}$$

$$\Gamma_{500} = A_0^5 + 10A_0^3\Gamma'_{200} + 5A_0\Gamma'_{400} + \Gamma_{52-1}\cos(2\xi_1 - \xi_2)$$

$$\Gamma'_{510} = (5/8)A_1^5 + (15/4)A_1^3A_2^2 + (15/8)A_1A_2^4$$

$$\Gamma_{510} = 5A_0^4A_1 + 10A_0^2\Gamma'_{310} + \Gamma'_{510}$$

$$\Gamma_{5-11} = 10A_0^3\Gamma_{2-11} + 5A_0\Gamma'_{4-11}$$

$$\Gamma_{53-1} = 5A_0\Gamma_{43-1}; \quad \Gamma_{5-32} = (5/8)A_1^3A_2^2$$

$$\Gamma_{520} = 5A_0^3A_1^2 + 5A_0\Gamma'_{420}; \quad \Gamma_{5-22} = 5A_0\Gamma_{4-22}; \quad \Gamma_{54-1} = (5/16)A_2A_1^4$$

$$\Gamma'_{530} = (5/16)A_1^5 + (5/4)A_1^3A_2^2; \quad \Gamma_{530} = 10A_0^2\Gamma_{330} + \Gamma'_{530}$$

$$\Gamma_{540} = 5A_0\Gamma_{440}.$$

Fourier coefficients of Φ^6:

$$\Gamma_{62-1} = 20A_0^3\Gamma_{32-1} + 6A_0\Gamma'_{52-1}; \quad \Gamma_{64-2} = (15/32)A_1^4A_2^2\cos(4\xi_1 - 2\xi_2)$$

$$\Gamma'_{600} = (5/16)(A_1^6 + A_2^6) + (45/16)A_1^2A_2^2(A_1^2 + A_2^2)$$

$$\Gamma_{600} = A_0^6 + 15A_0^4\Gamma'_{200} + 15A_0^2\Gamma'_{400} + \Gamma'_{600}$$
$$+ \Gamma_{62-1}\cos(2\xi_1 - \xi_2) + \Gamma_{64-2}\cos(4\xi_1 - 2\xi_2)$$

$$\Gamma_{610} = 6A_0^5A_1 + 20A_0^3\Gamma'_{310} + 6A_0\Gamma'_{510}$$

$$\Gamma'_{6-11} = (45/8)A_1^3A_2^3 + (15/8)A_1A_2(A_1^4 + A_2^4)$$

$$\Gamma_{6-11} = 15A_0^4\Gamma_{2-11} + 15A_0^2\Gamma'_{4-11} + \Gamma'_{61-1}$$

$$\Gamma'_{63-1} = (15/16)A_1^5A_2 + (15/8)A_1^3A_2^3; \quad \Gamma_{63-1} = 15A_0^2\Gamma_{43-1} + \Gamma'_{63-1}$$

$$\Gamma_{6-32} = 6A_0\Gamma_{5-32}$$

$$\Gamma'_{620} = (15/32)A_1^6 + (15/4)A_1^4A_2^2 + (45/16)A_1^2A_2^4$$

$$\Gamma_{620} = (15/2)A_0^4A_1^2 + 15A_0^2\Gamma'_{420} + \Gamma'_{620}$$

$$\Gamma'_{6-22} = (15/8)A_1^2A_2^2(A_1^2 + A_2^2); \quad \Gamma_{6-22} = 15A_0^2\Gamma_{4-22} + \Gamma'_{6-22}$$

$$\Gamma_{64-1} = 6A_0\Gamma_{54-1}$$

$$\Gamma_{630} = 20A_0^3\Gamma_{330} + 6A_0\Gamma'_{530}; \quad \Gamma_{6-33} = (5/8)A_1^3A_2^3; \quad \Gamma_{65-1} = (3/16)A_1^5A_2$$

$$\Gamma'_{640} = (3/16)A_1^6 + (15/16)A_1^4A_2^2; \quad \Gamma_{640} = 15A_0^2\Gamma_{440} + \Gamma'_{640}.$$

Fourier coefficients of Φ^7 (up to third order):

$$\Gamma'_{72-1} = (105/16)A_1^4A_2^3 + (105/64)A_1^6A_2 + (105/32)A_1^2A_2^5$$

$$\Gamma_{72-1} = 35A_0^4\Gamma_{32-1} + 21A_0^2\Gamma'_{52-1} + \Gamma'_{72-1}$$

$$\Gamma_{700} = A_0^7 + 21A_0^5\Gamma'_{200} + 35A_0^3\Gamma'_{400} + 7A_0\Gamma'_{600} + \Gamma_{72-1}\cos(2\xi_1 - \xi_2) + 7A_0\Gamma_{64-2}\cos(4\xi_1 - 2\xi_2)$$

$$\Gamma'_{710} = (35/64)A_1^7 + (105/16)A_1^5A_2^2 + (315/32)A_1^3A_2^4 + (35/16)A_1A_2^6$$

$$\Gamma_{710} = 7A_0^6A_1 + 35A_0^4\Gamma'_{310} + 21A_0^2\Gamma'_{510} + \Gamma'_{710}$$

$$\Gamma_{7-11} = 21A_0^5\Gamma_{2-11} + 35A_0^3\Gamma'_{4-11} + 7A_0\Gamma'_{6-11}$$

$$\Gamma_{73-1} = 35A_0^3\Gamma_{43-1} + 7A_0\Gamma'_{63-1}$$

$$\Gamma'_{7-32} = (105/64)A_1^5A_2^2 + (35/16)A_1^3A_2^4; \quad \Gamma_{7-32} = 21A_0^2\Gamma_{5-32} + \Gamma'_{7-32}$$

$$\Gamma_{75-2} = (21/64)A_1^5A_2^2$$

$$\Gamma'_{701} = (35/64)A_2^7 + (105/16)A_1^2A_2^5 + (315/32)A_1^4A_2^3 + (35/16)A_1^6A_2$$

$$\Gamma_{701} = 7A_0^6A_2 + 35A_0^4\Gamma'_{301} + 21A_0^2\Gamma'_{501} + \Gamma'_{701}$$

$$\Gamma_{720} = (21/2)A_0^5A_1^2 + 35A_0^3\Gamma'_{420} + 7A_0\Gamma'_{620}; \quad \Gamma_{7\text{–}22} = 35A_0^3\Gamma_{4\text{–}22} + 7A_0\Gamma'_{6\text{–}22}$$

$$\Gamma'_{74-1} = (105/64)A_1^4A_2^3 + (21/32)A_1^6A_2; \quad \Gamma_{74-1} = 21A_0^2\Gamma_{54-1} + \Gamma'_{74-1}$$

$$\Gamma_{7-43} = (35/64)A_1^4A_2^3$$

$$\Gamma'_{730} = (21/64)A_1^7 + (105/32)(A_1^5A_2^2 + A_1^3A_2^4)$$

$$\Gamma_{730} = 35A_0^4\Gamma_{330} + 21A_0^2\Gamma'_{530} + \Gamma'_{730}$$

$$\Gamma_{7-33} = 7A_0\Gamma_{6-33}; \quad \Gamma_{75-1} = 7A_0\Gamma_{65-1}.$$

Fourier coefficients of Φ^8 (up to third order):

$$\Gamma_{82-1} = 56A_0^5\Gamma_{32-1} + 56A_0^3\Gamma'_{52-1} + 8A_0\Gamma'_{72-1}$$

$$\Gamma'_{84-2} = (21/16)A_1^6A_2^2 + (35/16)A_1^4A_2^4; \quad \Gamma_{84-2} = 28A_0^2\Gamma_{64-2} + \Gamma'_{84-2}$$

$$\Gamma'_{800} = (35/128)(A_1^8 + A_2^8) + (35/8)A_1^2A_2^2(A_1^4 + A_2^4) + (315/32)A_1^4A_2^4$$

$$\Gamma_{800} = A_0^8 + 28A_0^6\Gamma'_{200} + 70A_0^4\Gamma'_{400} + 28A_0^2\Gamma'_{600} + \Gamma'_{800} + \Gamma_{82-1}\cos(2\xi_1 - \xi_2) + \Gamma_{84-2}\cos(4\xi_1 - 2\xi_2)$$

$$\Gamma_{810} = 8A_0^7A_1 + 56A_0^5\Gamma'_{310} + 56A_0^3\Gamma'_{510} + 8A_0\Gamma'_{710}$$

$$\Gamma'_{8-11} = (35/16)(A_1^7A_2 + A_2^7A_1) + (105/8)A_1^3A_2^3(A_1^2 + A_2^2)$$

$$\Gamma_{8-11} = 28A_0^6\Gamma_{2-11} + 70A_0^4\Gamma'_{4-11} + 28A_0^2\Gamma'_{6-11} + \Gamma'_{8-11}$$

$$\Gamma'_{83-1} = (21/16)A_1^7A_2 + (105/16)A_1^5A_2^3 + (15/4)A_1^3A_2^5$$

$$\Gamma_{83-1} = 70A_0^4\Gamma_{43-1} + 28A_0^2\Gamma'_{63-1} + \Gamma'_{83-1}$$

$$\Gamma_{8-32} = 56A_0^3\Gamma_{5-32} + 8A_0\Gamma'_{7-32}$$

$$\Gamma_{85-2} = 8A_0\Gamma_{75-2}; \quad \Gamma_{8-53} = (7/16)A_1^5A_2^3$$

$$\Gamma'_{820} = (7/16)A_1^8 + (105/16)A_1^6A_2^2 + (105/8)A_1^4A_2^4 + (35/8)A_1^2A_2^6$$

$$\Gamma_{820} = 14A_0^6A_1^2 + 70A_0^4\Gamma'_{420} + 28A_0^2\Gamma'_{620} + \Gamma'_{820}$$

$$\Gamma'_{8-22} = (105/32)A_1^2A_2^2(A_1^4 + A_2^4) + (35/4)A_1^4A_2^4$$

$$\Gamma_{8-22} = 70A_0^4\Gamma_{4-22} + 28A_0^2\Gamma'_{6-22} + \Gamma'_{8-22}$$

$$\Gamma_{84-1} = 56A_0^3\Gamma_{54-1} + 8A_0\Gamma'_{74-1}$$

$$\Gamma_{86-2} = (7/32)A_1^6A_2^2; \quad \Gamma_{8-43} = 8A_0\Gamma_{7-43}$$

$$\Gamma_{830} = 56A_0^5\Gamma_{330} + 56A_0^3\Gamma'_{530} + 8A_0\Gamma'_{730}$$

$$\Gamma_{8-12} = 56A_0^5\Gamma_{3-12} + 56A_0^3\Gamma'_{5-12} + 8A_0\Gamma'_{7-12}$$

$$\Gamma'_{8-33} = (35/16)A_1^3A_2^3(A_1^2 + A_2^2); \quad \Gamma_{8-33} = 28A_0^2\Gamma_{6-33} + \Gamma'_{8-33}$$

$$\Gamma'_{85-1} = (21/16)A_1^5A_2^3 + (7/16)A_1^7A_2; \quad \Gamma_{85-1} = 28A_0^2\Gamma_{65-1} + \Gamma'_{85-1}.$$

In the system of nonlinear equations (H) (see at the end), we use a few more coefficients which are not defined in the previous text. However, they can be easily determined using the following symmetry relations of Γ_{nlm}:

$$\Gamma'_{nlm}(A_1, A_2) = \Gamma'_{nml}(A_2, A_1). \tag{2a}$$

Hence, for either of l or $m \neq 0$,

$$\Gamma_{nlm}(A_0, A_1, A_2) = \Gamma_{nml}(A_0, A_2, A_1). \tag{2b}$$

Also

$$\Gamma_{n11}(A_0, A_1, A_2) = \Gamma_{n-11}(A_0, A_1, A_2), \tag{2c}$$

and

$$\Gamma_{n21}(A_0, A_1, A_2) = \Gamma_{n2-1}(A_0, A_1, A_2). \tag{2d}$$

Henceforth, the lower limit of summation over n is unity. Also,

$$\Gamma_{nlm} = 0 \text{ for } n < |l| + |m|.$$

Next, we denote the following terms:

$$N_{00} \equiv \sum \Gamma_{n00}/n! \tag{3a}$$

$$C_{1m} = \sum \Gamma_{nlm} \cos(l\xi_1 + m\xi_2)/n! \tag{3b}$$

$$S_{1m} \equiv \sum \Gamma_{nlm} \sin(l\xi_1 + m\xi_2)/n! \tag{3c}$$

(in the identities (3), the upper limit of summation is eight) and, in similar fashion, the next series of terms are defined as follows:

$$D_{c10} \equiv \sum A_1(\Gamma_{n00} - (1/2)\Gamma_{n20}) \cos(\xi_1)/n!$$

$$D_{s10} \equiv \sum A_1(\Gamma_{n00} - (1/2)\Gamma_{n20}) \sin(\xi_1)/n!$$

$$D_{c-11} \equiv \sum (A_2\Gamma_{n10} - (1/2)A_1\Gamma_{n01} - A_2\Gamma_{n-12}) \cos(\xi_2 - \xi_1)/n!$$

$$D_{s-11} \equiv \sum (A_2\Gamma_{n10} - (1/2)A_1\Gamma_{n01} - A_2\Gamma_{n-12}) \sin(\xi_2 - \xi_1)/n!$$

$$D_{c-32} \equiv \sum (A_2\Gamma_{n3-1} - (1/2)A_1\Gamma_{n-22} - A_2\Gamma_{n-33}) \cos(2\xi_2 - 3\xi_1)/n!$$

$$D_{s-32} \equiv \sum (A_2\Gamma_{n3-1} - (1/2)A_1\Gamma_{n-22} - A_2\Gamma_{n-33}) \sin(2\xi_2 - 3\xi_1)/n!$$

$$D_{c3-1} \equiv \sum (A_2\Gamma_{n-32} - (1/2)A_1\Gamma_{n4-1} - A_2\Gamma_{n30}) \cos(3\xi_2 - \xi_1)/n!$$

$$D_{s3-1} \equiv \sum (A_2\Gamma_{n-32} - (1/2)A_1\Gamma_{n4-1} - A_2\Gamma_{n30}) \sin(3\xi_2 - \xi_1)/n!$$

$$D_{c5-2} \equiv -A_2\Gamma_{65-1} \cos(5\xi_1 - 2\xi_2)/6!$$

$$D_{s5-2} \equiv -A_2\Gamma_{65-1} \sin(5\xi_1 - 2\xi_2)/6!$$

$$D_{c01} \equiv \sum (2\Gamma_{n00} - \Gamma_{n02})A_2 \cos(\xi_2)/n!$$

$$D_{s01} \equiv \sum (2\Gamma_{n00} - \Gamma_{n02})A_2 \sin(\xi_2)/n!$$

$$D_{c20} \equiv \sum[(1/2)A_1(\Gamma_{n10} - \Gamma_{n30}) - A_2\Gamma_{n21}]\cos(2\xi_1)/n!$$

$$D_{s20} \equiv \sum[(1/2)A_1(\Gamma_{n10} - \Gamma_{n30}) - A_2\Gamma_{n21}]\sin(2\xi_1)/n!$$

$$D_{c4-1} \equiv \sum[(1/2)A_1(\Gamma_{n3-1} - \Gamma_{n5-1}) - A_2\Gamma_{n40}]\cos(4\xi_1 - \xi_2)/n!$$

$$D_{s4-1} \equiv \sum[(1/2)A_1(\Gamma_{n3-1} - \Gamma_{n5-1}) - A_2\Gamma_{n40}]\sin(4\xi_1 - \xi_2)/n!$$

$$D_{c-22} \equiv \sum[(1/2)A_1(\Gamma_{n-32} - \Gamma_{n-12}) - A_2\Gamma_{n-23}]\cos(2\xi_2 - 2\xi_1)/n!$$

$$D_{s-22} \equiv \sum[(1/2)A_1(\Gamma_{n-32} - \Gamma_{n-12}) - A_2\Gamma_{n-23}]\sin(2\xi_2 - 2\xi_1)/n!$$

$$D_{c-43} \equiv -(1/2)A_1\Gamma_{6-33}\cos(3\xi_2 - 4\xi_1)/6!$$

$$D_{s-43} \equiv -(1/2)A_1\Gamma_{6-33}\sin(3\xi_2 - 4\xi_1)/6!.$$

(In the previous set of identities, the upper limit of summation is six.)

Applying the principle of harmonic balance method in eq. (1) and applying all the identities mentioned in this appendix, we derive the following set of five coupled nonlinear algebraic equations of the unknown variables (A_0, A_1, A_2, ξ_1, ξ_2). The equations are written below [from eqs (H_1) to (H_5)]:

$$F_1 \equiv N_{00} - (1/2)(C_{10} + C_{-11} + C_{3-1} + C_{-32} + C_{5-2} + C_{-53}) = 0 \qquad (H_1)$$

$$\begin{aligned} F_2 \equiv\ & -\omega^2 A_1 \sin(\xi_1) \\ & + \alpha\omega[A_1\cos(\xi_1) + c(D_{C10} + D_{C-11} + D_{C-32} + D_{C3-1} + D_{C5-2})] \\ & + [S_{10} + S_{-11} + S_{3-1} + S_{-32} + S_{5-2} + S_{-53} \\ & \quad - (m/2)(S_{01} + S_{20} + S_{-22} + S_{4-1} + S_{-43} + S_{6-2})] \\ & - f\sin(\vartheta) = 0 \end{aligned} \qquad (H_2)$$

$$\begin{aligned} F_3 \equiv\ & -\omega^2 A_1 \cos(\xi_1) \\ & - \alpha\omega[A_1\sin(\xi_1) + c(D_{S10} + D_{S-11} + D_{S-32} + D_{S3-1} + D_{S5-2})] \\ & + [C_{10} + C_{-11} + C_{3-1} + C_{-32} + C_{5-2} + C_{-53} \\ & \quad - (m/2)(2N_{00} + C_{01} + C_{20} + C_{-22} + C_{4-1} + C_{-43} + C_{6-2})] \\ & - f\cos(\vartheta) = 0 \end{aligned} \qquad (H_3)$$

$$
\begin{aligned}
F_4 \equiv\ & -4\omega^2 A_2 \sin(\xi_2) \\
& + \alpha\omega[2A_2\cos(\xi_2) + c(D_{C01} + D_{C20} + D_{C4-1} + D_{C-22} + D_{C-43})] \\
& + [S_{01} + S_{20} + S_{-22} + S_{4-1} + S_{-43} + S_{6-2} \\
& \quad - (m/2)(S_{10} + S_{-11} + S_{3-1} + S_{-32} + S_{5-2} + S_{-53} + S_{30} + S_{11} \\
& \quad + S_{-12} + S_{5-1} + S_{-33})] = 0 \qquad (\mathrm{H}_4)
\end{aligned}
$$

$$
\begin{aligned}
F_5 \equiv\ & -4\omega^2 A_2 \cos(\xi_2) \\
& - \alpha\omega[2A_2\sin(\xi_2) + c(D_{S01} + D_{S20} + D_{S4-1} + D_{S-22} + D_{S-43})] \\
& + [C_{01} + C_{20} + C_{-22} + C_{4-1} + C_{-43} + C_{6-2} \\
& \quad - (m/2)(C_{10} + C_{-11} + C_{3-1} + C_{-32} + C_{5-2} + C_{-53} + C_{30} + C_{11} \\
& \quad + C_{-12} + C_{5-1} + C_{-33})] = 0. \qquad (\mathrm{H}_5)
\end{aligned}
$$

References

[1] G Contopoulos and C Polymilis, *Physica* **D24**, 328 (1987)

[2] M Toda, *Supp. Prog. Phys.* **45**, 174 (1970)

[3] I Birol and A Hacinliyan, *Phys. Rev.* **E52**, 4750 (1995)

[4] L Zachilas, *Int. J. Bifurcat. Chaos* **20**, 3007, 3391 (2010)

[5] S Udry and L Martinez, *Physica* **D24**, 328 (1987)

[6] S Habib, H E Kandrup and M E Mahon, *Phys. Rev.* **E53**, 5473 (1996); *Astrophys. J.* **480**, 155 (1997)

[6a] The class of oscillators with the restoring force $\left[(\exp(\Phi) - 1) = \sum_{n=1}^{\infty} \Phi^n/n!\right]$ has been referred to as 'Toda oscillator' by Oppo and Politi [7] while reducing the oscillator form of two-level rate-equation model [8] of class-B lasers (e.g., CO_2, Nd-YAG, semiconductor and fibre lasers). Later, others have followed the same convention [9–13]. All known experimentally observed salient features of these lasers, including various harmonic and subharmonic resonances, generalized multistability, various forms of crises and intermittency have been nicely explained by the rate equations or its Toda oscillator form.

[6b] The categorization of soft-spring and hard-spring bistabilities has been made following the convention of mechanical oscillatories [14].

[7] G-L Oppo and A Politi, *Z. Phys.* **B59**, 111 (1985)

[8] M Surgent III, M O Scully and W E Lamb Jr, *Laser physics* (Addison-Wesley, London, 1974) Chapter 8, pp. 96–113

[9] U Parlitz and W Lauterborn, *Phys. Lett.* **A107**, 351 (1985)
T Kurz and W Lauterborn, *Phys. Rev.* **A37**, 1029 (1988)
W Lauterborn and R Steinhoff, *J. Opt. Soc. Am.* **B5**, 1097 (1988)

[10] G-L Oppo, J R Tredicce and L M Narducci, *Opt. Commun.* **69**, 393 (1989)

[11] C Scheffczyk, U Parlitz, T Kurz, W Knop and W Lauterborn, *Phys. Rev.* **A43**, 6495 (1991)
U Parlitz, *Int. J. Bifurcat. Chaos* **3**, 703 (1993)

[12] B K Goswami, *Phys. Lett.* **A190**, 279 (1994); *Opt. Commun.* **122**, 189 (1996); *Int. J. Bifurcat. Chaos* **12**, 2691 (1997); *Phys. Lett.* **A245**, 97 (1998); *Phys. Rev.* **E62**, 2068 (2000)

[13] B K Goswami, *Rivista del Nuovo Cimento* **28**, 1 (2005)

[14] A H Nayfeh and D T Mook, *Nonlinear oscillations* (Wiley, New York, Chichester, Brisbane, Toronto, Singapore, 1979)

[15] Ch Hayashi, *Nonlinear oscillations in physical systems* (McGraw-Hill, New York, San Francisco, Toronto, London, 1964)

[15a] Please see Appendix and in particular, the system of nonlinear algebraic equations (eqs H_1 to H_5).

[15b] For increased driving amplitude, the magnitude of Φ could be larger than unity. In such cases, the progressive decrease of the effect of higher-order nonlinear terms should occur in the asymptotic limit.